Published on Engineering Geology, doi: 10.1016/j.enggeo.2018.10.008

Using ambient noise to characterise seismic slope response: the case of Qiaozhuang peri-urban hillslopes (Sichuan, China)

Del Gaudio Vincenzo[a,b], Luo Yonghong[b], Wang Yunsheng[b], Wasowski Janusz[c]

[a] Dipartimento di Scienze della Terra e Geoambientali, Università degli Studi di Bari "Aldo Moro", Italy

[b]State Key Laboratory of Geo-Hazard Prevention and Geo-Environment Protection, Chengdu University of Technology, P.R. China.

[c]Consiglio Nazionale delle Ricerche – Istituto di Ricerca per la Protezione Idrogeologica, Bari, Italy.

ABSTRACT

The Mw 7.9 Wenchuan earthquake of May 12th, 2008 shattered and induced failures on hillslopes surrounding the centre of the town of Qiaozhuang, located 250 Km NE of the mainshock epicentre. This motivated investigations on the possible occurrence of site amplification phenomena. The initial efforts involved a temporary accelerometer monitoring carried out between April and October 2009 on Weigan hill and Mount Dong, located SW and NE of the Qiaozhuang centre, respectively. The monitoring results revealed that the local geological setting, characterised by Silurian phyllites with sub-vertical schistosity (at Weigan) and by fractured Precambrian limestones (at Dong), exert major influence on the slopes resonance phenomena, with a secondary contribution due to the topographic setting. To extend the investigation on local slope response, a series of ambient noise recordings were conducted at several sites of the two hills, as well as at Mount Shizi (located NW of the town centre), which is topographically and geologically similar to Mount Dong. The focus was on the sites monitored by accelerometer stations, whose seismic records provided the opportunity to validate the outcomes of ambient noise analysis. Noise data were analysed using two approaches: the standard Nakamura's method and a new technique based on analysis of instantaneous polarization properties, aimed at estimating ellipticity of Rayleigh waves. Data interpretation was hampered by a contingent factor, i.e. environmental conditions characterised by a strong persistent E-W polarized noise at low frequencies (below 1 Hz), and by the complex of geologic and geomorphic conditions. The latter, particularly in the case of Weigan hill, appear responsible for a considerable amplification of vertical ground motions. The repeated recordings and the comparison of the outcomes of the two techniques of noise analysis with the accelerometer data showed that the new technique provides more stable and consistent results. Furthermore, the new technique was able to reveal site resonance properties that Nakamura's method fails to recognise because of transient overlapping of different type waves. Overall, the ambient noise analysis provided evidence of i) low frequency resonance (~1 Hz) acting at the scale of the entire relief (on Weigan Hill), ii) directional amplifications at intermediate frequencies (~4 Hz) affecting ridge crests made of fractured limestone (on Mounts Dong and Shizi), and iii) higher frequency resonances (7-20 Hz), which vary at a very local scale. This information is relevant for inferring the susceptibility of local slopes to earthquake-induced failures, and hence for the collateral seismic hazard assessment in the Qiaozhuan peri-urban areas.

Keywords: seismic slope response; ambient noise; seismically induced landslides; 2008 Wenchuan earthquake; China.

1. Introduction

The 2008 Wenchuan earthquake (7.9 Mw), occurred in the Sichuan Province, China, was responsible for over 87000 victims (Qi et al., 2010; Fan et al., 2018). A substantial percentage of this heavy toll was due to the widespread slope failures that affected the mountainous Longmenshan region, along the eastern margin of the Tibetan plateau, and, in some cases, involved urban areas at the foot of steep slopes (Fan et al., 2018 and references therein).

Many landslides originated near ridge crests, which suggested a possible role of topographic amplification in favouring slope failures (Wang et al., 2012), in analogy with what had been indicated for other seismic events (e.g., Harp and Jibson, 2002; Sepúlveda et al., 2005; Meunier et al., 2008). This motivated subsequent investigations including also strong motion monitoring with temporary arrays of accelerometers (e.g., Luo et al., 2014). One of the investigated areas is the town of Qiaozhuang, capital of the Qingchuan County. This town is located about 250 km NE of the mainshock epicentre, but very close to the epicentre of the strongest aftershock (6.1 Mw) of the Weinchuan earthquake sequence. The aftershock occurred on 25 May 2008 about 20 km east of the town and was likely due to the activation of a branch of the Qingchuan-Pingwu fault system, which passes through the Qingchuan County.

Field investigations revealed that the mainshock of 12 May 2008 induced ground fissures and rock falls in the peri-urban area of Qiaozhuang (Liu et al., 2009; Luo et al., 2014). The failures originated mainly in the upper parts of rock ridges at Weigan hill, located to the SW of the urban area, Mount Shizi to the NW and Mount Dong to the NE (Fig. 1). Slope monitoring of Weigan hill, set up following the mainshock, revealed that the 25 May 2008 aftershock aggravated the earlier slope instabilities (Sheng et al., 2009). Therefore, there was much concern about the safety of the Qiaozhuang built-up areas located at the foot of the three ridges, especially in relation to the possible effect of other large magnitude earthquakes. There was fear that such events could trigger landslides damming the river that flows through the town.

Accelerometer stations were setup at the three Qiaozhuang ridges to investigate the possible presence of site amplification that could favour landslide mobilization. Accelerometers recorded mostly minor events of the Wenchuan seismic sequence from April to October 2009, with a maximum magnitude 5.3 Mw for an event occurred on 30 June (29 June according to the GMT system). The analysis of the recordings suggested the presence of directional maxima in ground shaking, possibly due to directional resonance phenomena controlled by local geologic structures (Luo et al., 2014). However, the limited number of the recorded seismic events, as well as their azimuthal distribution concentrated along the Qingchuan-Pingwu fault system strike, resulted in uncertain interpretation of the observed directivity, i.e., whether it actually reflects the site dynamic response or depends on source properties. Therefore, we conducted supplementary investigations using techniques based on ambient noise analysis, which, in last two decades, have had a growing employment in the study of landslide-prone slopes (cf. Gallipoli et al., 2000; Havenith et al., 2002; Méric et al., 2007; Danneels et al., 2008; Jongmans et al., 2009; Burjánek. et al., 2010; Moore et al., 2011).

While procedures for drawing information on site response from ambient noise are well established for plain site conditions (flat horizontal layering: see Bard and the SESAME Team, 2004), more problematic is the case of sites having pronounced topographic relief, complex geology and spatially variable rock mechanical properties (Del Gaudio et al., 2008; 2013; 2014). Indeed, standard noise analysis techniques like Nakamura's method (Nakamura, 1989) have limited efficacy even in identifying resonance frequencies (which is generally considered to be a reliable outcome of this technique) when amplification acts at multiple frequencies and with a pronounced directional variation, as frequently observed in complex site conditions (Del Gaudio et al., 2008; Del Gaudio, 2017).

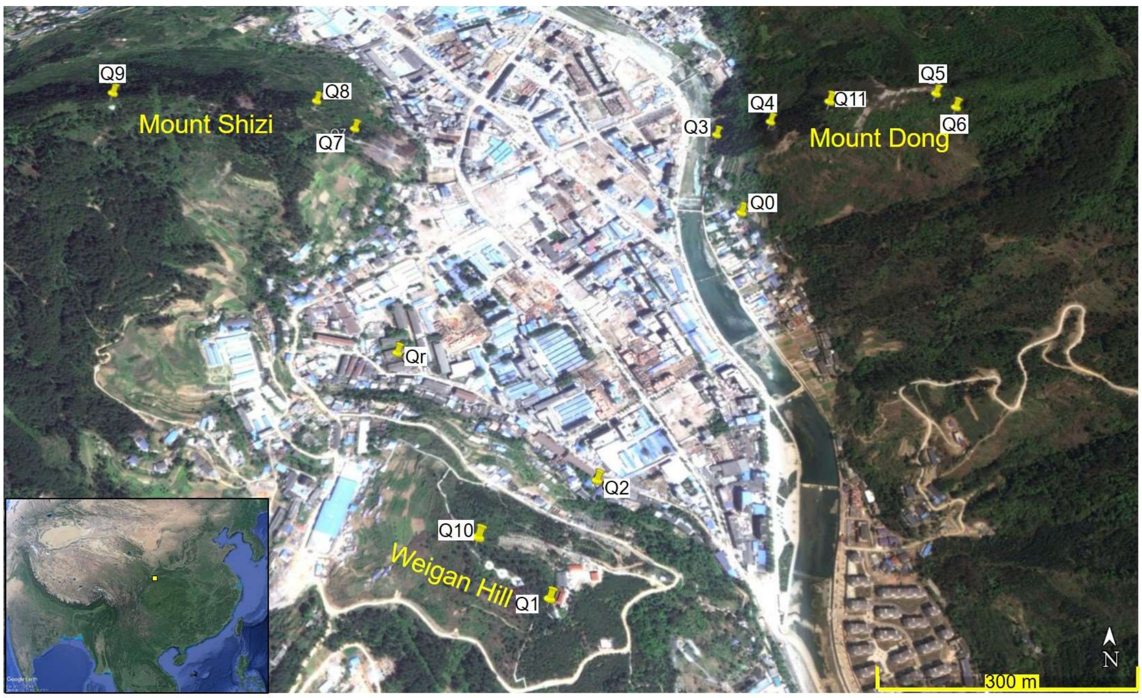

Fig. 1: Google Earth^{TM} image of 2010 of the urban area of Qiaozhuang and locations of the investigated sites: Q1-11 mark noise recording sites and Qr is a reference site; Q0 is the site of the accelerometer station used as reference for the analysis of seismic recordings acquired on Weigan Hill and discussed in Luo et al. (2014). The yellow dot in the inset shows the geographic location of the study area.

The main objective of this work is to present new results of ambient noise analysis, which lead to the improved comprehension of dynamic response of the hills around Qiaozhuang. We conducted noise recordings during two measurement campaigns in a dozen of sites (from Q1 to Q11 and the reference station Qr: see Fig. 1), which included the sites of accelerometer stations establihed after the 2008 Wenchuan event. Data analysis took advantage of the advanced technique of ambient noise analysis, recently developed and successfully tested by one of us (Del Gaudio, 2017). For comparative purposes, the same noise data were analysed using the standard Nakamura technique. Finally, the outcomes of the analysis of ambient noise and seismic recordings were compared to provide additional constraints on data analysis and results interpretation.

2. Geological setting

The area studied is located in the NE part of the Sichuan Province, forming the northern part of the tectonically active Longmenshan mountain belt. The local tectonic setting is complex with the urban/periurban area of Qiaozhuang traversed by the major Qingchuan-Pingwu fault zone. The tectonic structure has approximately ENE trend and steeply dips to the north. It is composed of three sub-parallel fault branches (Fig. 2).

Liu et al., (2009) reported indications of significant activity along the Qingchuan-Pingwu fault from the Late Pleistocene to Early Holocene. Thrusting and associated strike-slip faulting represent the dominant deformation mechanism with the estimated average displacement rate ranging from 0.6 to 1.2 mm/year. In the two years following the 2008 Wenchuan earthquake mainshock, over 2000 aftershocks (with magnitude up to a maximum of 6.1) have been registered in the vicinity of the Qingchuan-Pingwu fault zone (Liu et al., 2009).

The rocks in the study area are intensely sheared because of the long history of tectonic activity. The principal lithologic units are shown in Fig.2. These include: limestones of Upper Sinian age, phyllites (Lower Silurian), and also sandstones (Lower Sinian) in the northermost periphery of the Qiaozhuang urban area.

Although good outcrops are limited because of the presence of dense vegetation, it is clear that the different rock units are tectonically juxtaposed (cf. Fig. 2). In particular, the limestones appear to be thrust over the phyllites at Mount Dong. However, the presence of approximately E-W oriented strike-slip shears (horizontal striations), as well as fault breccia observed at Mount Dong's limestone outcrops, indicate that the local structural setting is more complex. In addition to the approximately E-W oriented shears, the limestone seems affected by the following fracture sets: one trending NW-NNW and dipping about 75° to SW, and the other striking NNE and dipping about 65° to SE.

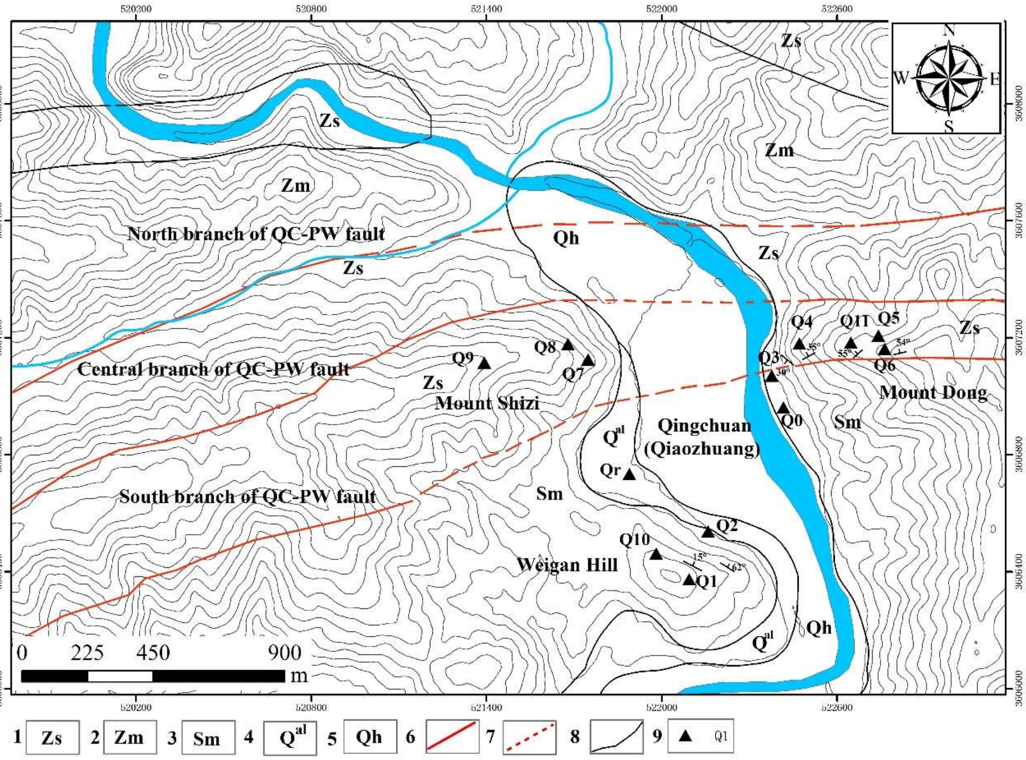

Fig. 2. Geologic sketch map of the Qiaozhuang town area, Qingchuan County: 1 – Zs, Upper Sinian (limestone); 2 – Zm, Lower Sinian (sandstone); 3 – Sm, Lower Silurian (phyllite); 4 – Q^{al}, Quaternary (alluvium); 5 – Qh, Quaternary–Holocene (alluvial deposits); 6 – Qingchuan–Pingwu Fault composed of three branches (north, central and south); 7 – Inferred fault trend; 8 – Lithostratigraphic boundary; 9 – Noise and seismic recording stations (modified after Liu et al., 2009).

In general, the outcrops are even more limited at Mount Shizi. Nevertheless, fractured limestone crops out at the station Q7 and the presence of limestone bedrock was revealed thanks to the excavations of shafts that host stations Q8 and Q9. This indicates that the structural setting of Mount Shizi bears considerable similarity with that of Mount Dong, where the stations located at the upper part of the ridge (Q4, Q5, Q6 and Q11) are sited on fractured limestone bedrock, whereas the topographically lower stations (Q0 and Q3) are located on the phyllites.

Regarding the Weigan Hill, the bedrock appears to be made mainly of phyllites (Fig. 2). Again, the outcrops are limited, but the artificial cut near the station Q1 showed that the phyllites are weathered and have sub-vertical schistosity, apparently sub-parallel to the elongation direction (NW) of the ridge.

3. Data acquisition

Ambient noise recordings were carried out using a couple of tromographs Tromino. These “all-in-one” instruments include, within a box of 10x14x8 cm, a 3-component electrodynamic velocimeter with high sensitivity (10^{-6} mm/s) and full scale of ±1.2 mm/s, together with an acquisition system, powered by a couple of AA batteries (see http://moho.world/en/tromino/ for details). The sensors have a relatively homogeneous response in a frequency interval between 0.5 to 20 Hz and, in the same frequency band, a self-noise largely below the level of ambient noise.

Noise measurements were conducted keeping one tromograph in continuous recording at a “reference” station, while the other was moved from one measurement site to the other. Noise recordings were acquired through sessions of 46 minutes, during the first campaign (17-18 May 2013), reduced to 30 minutes in the second one (20 June 2017). This data acquisition scheme allows controlling possible time variations of noise wave-field generation (during a campaign and between different campaigns), which could be misinterpreted as spatial variation of the dynamic response at sites where data are acquired at different times. Furthermore, in order to recognise the occurrence of directional resonance, it was essential to verify whether directional maxima of noise amplitude are a persistent feature, specific of an investigated site, or whether they reflect occasional polarizations controlled by noise source. Therefore, the measurements were repeated at two distinct campaigns with different environmental conditions.

Station named Qr was chosen as reference for both measurement campaigns. The station is located on the flat ground made of alluvial deposits, at the eastern periphery of the urban area, distant from the road traffic (Figs. 1, 2). This site, however, may not be considered a reference station in the strict sense of the term used for earthquake recording comparisons (a term that indicates a site free from amplification, typically located on stiff rocks). Nevertheless, through continuous recordings at Qr we could verify whether variations in noise wave-field energization can be responsible of differences observed among recordings at different stations. The other measurement points were mostly located at the sites of the accelerometer stations; some of these provided recordings of seismic events of the Wenchuan sequence between April and October 2009.

The location of the measurement points is shown in Figs. 1-2. On Weigan hill, recordings were acquired at three sites named Q1, Q2 and Q10. The first station was located at the site of a free field accelerometer station near the Bao Lian Temple, about 20 m below the hill top. While at this station noise data were acquired during both the campaigns of 2013 and 2017, just one recording was carried out at the other two stations: at Q2, located inside a building at the foot of Weigan hill, only in 2013, and at Q10, at the top of the hill, only in 2017. Accelerometer recordings of seismic events at Q1 and Q2 were subject of a detailed analysis in a previous paper (Luo et al., 2014).

On Mount Dong, five recording stations, named Q3, Q4, Q11, Q5 and Q6, were sited at increasing elevations (between about 800 and 950 m a.s.l.) along an approximately east-west oriented ridge (Fig. 1). Q3 was located at the foot of the relief, near the river, not far from the seismic station Q0, which Luo et al. (2014) adopted as reference for the analysis of seismic recordings. Noise was recorded in both measurement campaigns at Q3, Q4 and Q5, whereas at Q6 and Q11 data were acquired only in 2013 and in 2017, respectively.

On Mount Shizi, noise data were obtained in both measurement campaigns in three stations, named Q7, Q8 and Q9. The stations were located at increasing elevations, from 870 to 980 m a.s.l., on an east-west ridge almost aligned with that of Mount Dong, but on the opposite side of the Qiaozhuang river valley.

4. Analysis methodology

Noise recordings were analysed using two different techniques. The first is the standard Nakamura's method (Nakamura, 1989), applied according to the guidelines provided by Bard and the SESAME Team (2004). Noise recordings were subdivided into time windows of 20 s, excluding those with spectra strongly differing from the average of the others. For each window, the spectra of the three components were smoothed using the function proposed by Konno and Ohmachi (2008); then, the spectral ratios H/V between horizontal and vertical components were calculated and the results were averaged over the different time windows. In order to examine the directional variation of the horizontal-to-vertical noise ratios (HVNR), horizontal components were calculated for different azimuths, spaced by 10°.

It is generally reckoned that site resonance frequencies can be identified from pronounced peaks in the curve of spectral ratios plotted as function of frequency. Typically, a peak appears where a surface horizontal layer has a strong contrast of seismic impedance (the product of density times S-wave velocity) in comparison to a stiffer substratum. In principle, the amplification factor could be inferred from the amplitude of the HVNR peak, since these two quantities, both controlled by the local impedance contrast, are correlated. However, difficulties arise because the peak amplitude can considerably vary according to the proportion of different type of waves contributing to the noise (Rayleigh, Love and body waves: cf. Bonnefoy-Claudet et al., 2006). Considering this and in an effort to draw more information from noise analysis, we also used the so-called HVIP technique (horizontal-to-vertical ratio from instantaneous polarization) developed by Del Gaudio (2017). This technique isolates, within noise recording, wave packets of a single type, in particular Rayleigh waves, whose properties can be interpreted in terms of subsoil characteristics controlling the site dynamic response.

The HVIP method consists of applying an analytic transformation to the noise recording, so that noise polarization properties can be identified instant by instant. It allows representing ground motion as the projection onto the real space of a complex vector whose amplitude changes relatively slowly in time, outlining the recording envelope, whereas ground motion varies more rapidly as effect of phase variations.

Morozov and Smithson (1996) showed that ground motion can be described at each instant as following an elliptical trajectory whose principal axes can be determined. Thus, the HVIP method analyses instantaneous polarization properties of noise to identify wave packets showing a Rayleigh-type polarization, i.e., characterised by an elliptical particle motion lying on a vertical plane with principal axes oriented according to horizontal and vertical directions.

Once these parts of the recording are isolated, the analytic transformation is applied to the two horizontal components to determine direction and amplitude of maximum ground motion $H_{max}(t)$ on the horizontal plane, and, separately, to the vertical component to determine its instantaneous amplitude $V(t)$. In this way, the ratio H_{max}/V provides an instantaneous estimate of the Rayleigh wave ellipticity, cleaned from the contamination of other wave types.

The diagram of Rayleigh wave ellipticity versus frequency shows a peak at the site resonance frequency (cf. Bard, 1999) and its amplitude depends on the impedance contrast between surface layers and bedrock. Thus, such a diagram can provide information on site response properties. For this purpose, the outlined procedure is applied to time series obtained passing noise recording through narrow-band filters centred on different central frequencies f_c. The curve of mean ellipticity values resulting from each time series, plotted as function of f_c, provides an estimate of the Rayleigh wave ellipticity dependence on frequency. To improve the spectral resolution, f_c values with small spacing (e.g., 0.05 Hz) can be selected and the resulting ellipticity curve can then be smoothed through the Konno and Ohmachi (2008) function. More details on the methodology can be found in Del Gaudio (2017).

5. Results

5.1 Reference site

Figures 3 and 4 report the results of the analysis of noise recordings acquired at the reference station Qr during the two measurement campaigns and processed through both the standard Nakamura technique (HVNR values) and the approach based on instantaneous polarization analysis (HVIP values). Polar diagrams show the spectral ratio H/V (for Nakamura's method – Fig. 3) or the Rayleigh wave ellipticity (for the HVIP method – Fig. 4) as function of azimuth and frequency. Single diagrams are relative to time spans during which noise was simultaneously recorded at Qr and at one of the other stations (indicated in the diagram header). The comparative analysis of these results provides an insight into the different performance of the two analysis methods. Figures 3 and 4 show that the two techniques are consistent in identifying a significant site resonance at a frequency around 5 Hz. The HVNR method seems to have a better resolving power than HVIP, providing sharper peaks (see Fig. 5): analysing different time intervals, the former technique gave estimates of resonance frequencies from 4.95 to 5.40 Hz, whereas the latter from 4.75 to 5.95. However, the average values calculated on long data acquisition are practically the same (5.20 against 5.25 Hz), which implies that reliable frequency estimates can be obtained with the HVIP technique as well, using longer data acquisitions than those required by the Nakamura's method.

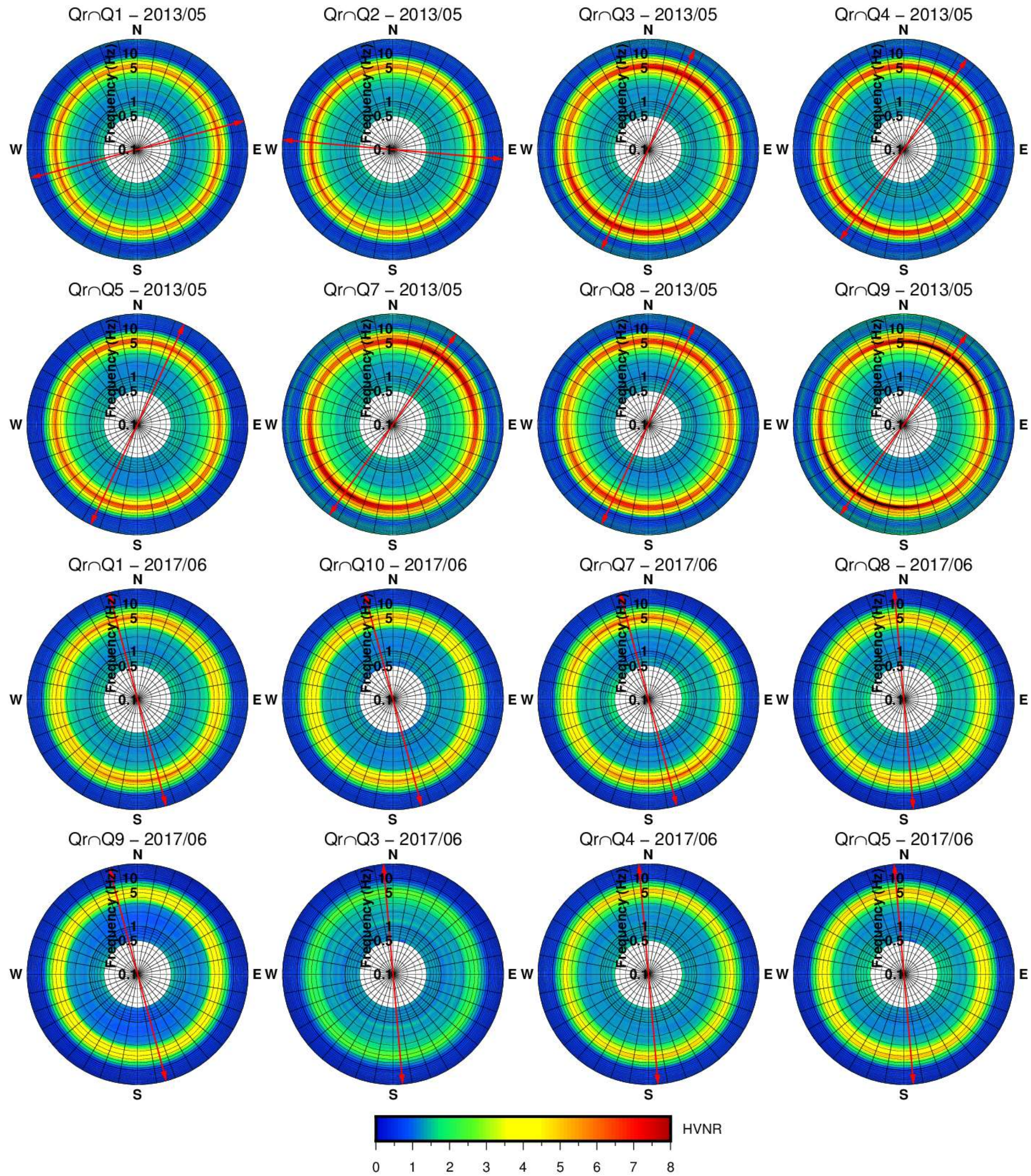

Fig. 3: Polar diagrams showing the results of the analysis of noise recorded at the reference station Qr, using the Nakamura's method. Spectral ratios are plotted through a colour scale as function of frequency (reported radially) and azimuth. Red arrows mark the direction of maximum spectral ratio. Different diagrams are relative to time intervals of Qr noise recordings, during which ambient noise was recorded also at another station (as indicated in the header of each diagram). Diagrams are arranged in chronological order from left to right and from top to bottom: the first eight diagrams are relative to the first measurement campaign (May 2013), the others are relative to the second campaign (June 2017).

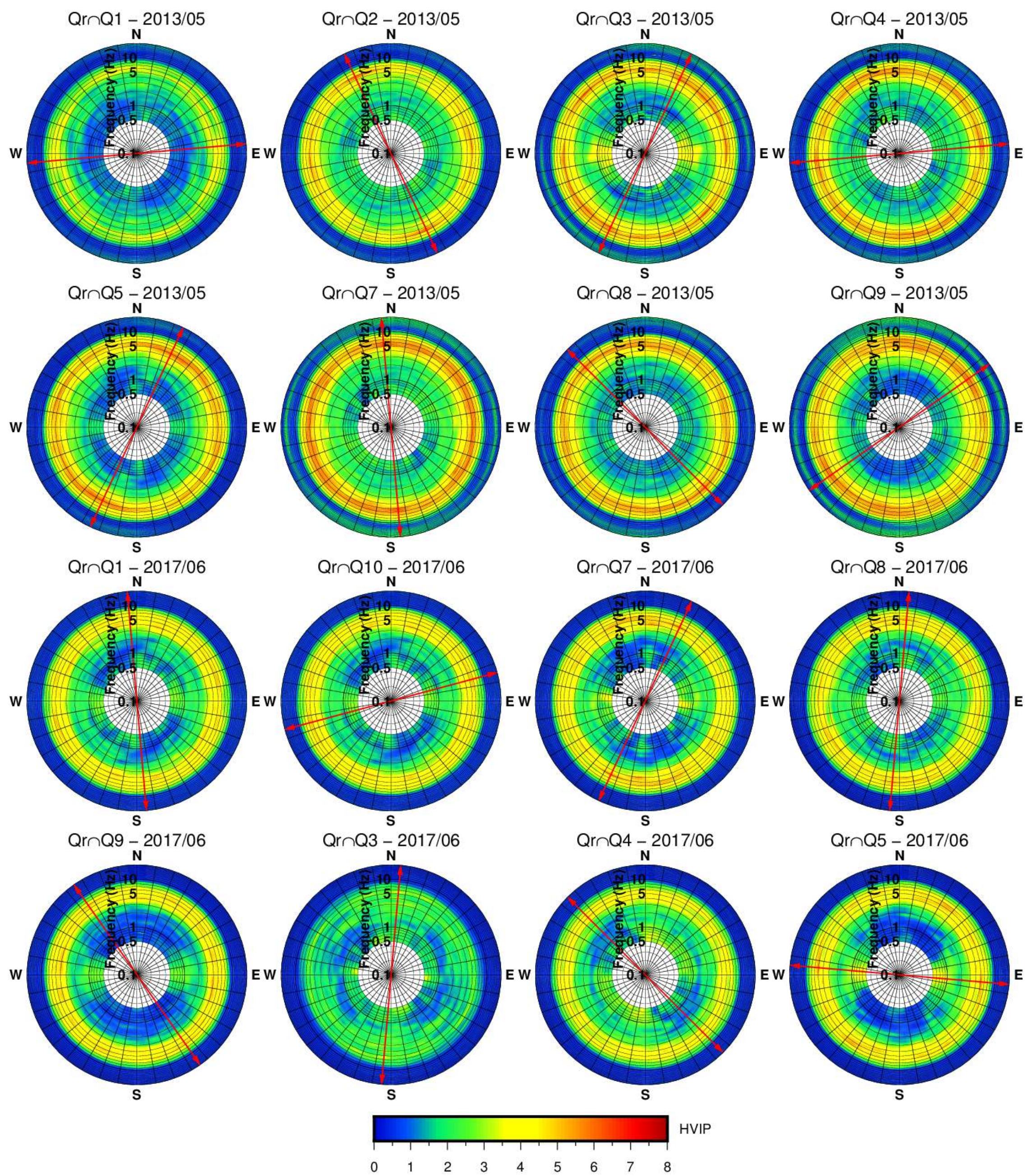

Fig. 4: Polar diagrams showing the results of the analysis of noise recorded at the reference station Qr, using the HVIP method. Red arrows mark the direction of maximum Rayleigh wave ellipticity. Different diagrams are relative to different time intervals of Qr noise recordings, during which ambient noise was recored also at another station (as indicated in the header of each diagram). Diagrams are arranged in chronological order from left to right and from top to bottom: the first eight diagrams are relative to the first measurement campaign (May 2013), the others are relative to the second campaign (June 2017).

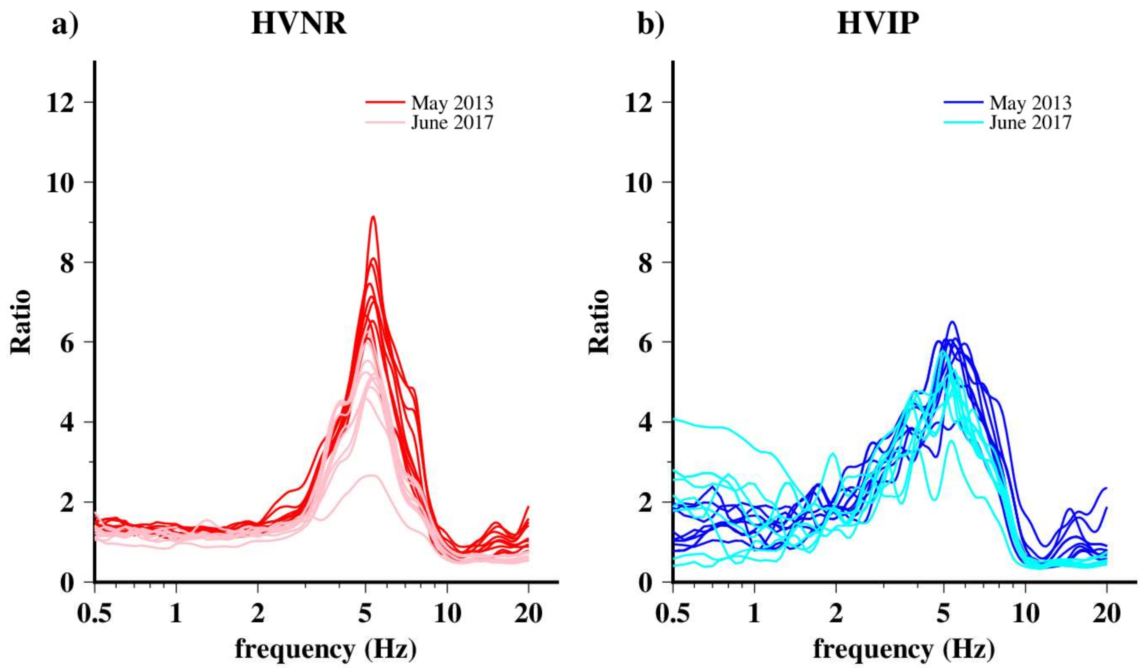

Fig. 5: Curves of spectral ratios obtained with the Nakamura's method (a) and of Rayleigh wave ellipticity estimated by applying the HVIP technique (b) for the reference station Qr, along the direction that, at different time intervals, provided a maximum (see red arrows in Figs 2 and 3). In each diagram, two different colour shades distinguish the results relative to the measurement campaigns of May 2013 and June 2017.

Figures 3 and 4 show no evidence of a preferential directivity in site response at reference Qr. Both HVNR and HVIP diagrams show directional maxima (marked by red arrows in Figs 3 and 4) changing from one time interval to the other, sometimes with an abrupt rotation of the orientation between even temporally close recordings.

The amplitude of the maxima also shows some variability (see Fig. 5), which represents an important factor of uncertainty in data interpretation. Indeed, this amplitude can correlate with the contrast of impedance between the surface layer and the substratum, which also controls the amplification factor. Although the HVIP method shows a stronger variability than HVNR in estimating the low ellipticity values at frequencies far from the resonance one, the estimate of peak values appears more stable than that in the case of the HVNR method. The HVNR peak values show a more pronounced scattering, from 2.7 to 9.1, in comparison to the HVIP peaks (between 3.5 and 6.5. This difference is reflected by standard deviation, which for HVNR is almost twice that of HVIP (1.5 against 0.8). Even the mean values appear quite different, being 6.2 for HVNR and 5.4 for HVIP.

The wider variability of HVNR finds an explanation in the observation, reported by Del Gaudio (2017), that only a small percentage (in the order of 1-2 %) of the noise recordings shows a clear Rayleigh-type polarization and is, therefore, selected for HVIP calculations. This is likely because other kinds of waves are constantly overlapped to Rayleigh waves and only when more energetic wave packets of this type (typically just for some tens of seconds) arrive at the sensor, a clear elliptical particle motion lying in a vertical plane can be recognised.

As a consequence, HVNR peak values, calculated as average spectral ratios on time windows of 20-30 s, are strongly influenced by the mixing of waves, some of which (e.g., Love waves) can considerably increase the H/V spectral ratios, whereas others (e.g., strong P-waves impinging the surface along sub-vertical direction) can reduce them. Thus, according to the amount of different types of waves contributing to the noise wave-field, which can change instant by instant depending on temporary source excitation, HVNR values can exhibit a strong variability. The HVIP method, selecting a single type of waves, provides more stable results.

The greater stability of HVIP results is further confirmed by a comparison of the results obtained in the two measurement campaigns: while HVIP provided relatively similar estimates of peak amplitude (5.84±0.72 in 2013 and 5.06±0.67 in 2017), the difference between HVNR maxima estimates was much higher (7.35±0.94 in 2013 and 5.05±1.03 in 2017).

HVIP data suggest the possible occurrence of a change in site conditions, which may have modified Rayleigh wave properties, slightly decreasing their ellipticity. We speculate that this variation can occur, for instance, in relation to changes of soil water content, which modify soil Poisson ratio. However, the variation in peak amplitude appears limited. In case of HVNR the variation is much stronger, likely because being additionally influenced by different conditions of noise wave-field energization, with a different proportion of contributing wave types. Therefore, interpretations of HVNR curves aimed at inferring sub-soil velocity models (cf., Castellaro and Mulargia, 2009), assuming that they reflect Rayleigh wave ellipticity, should be regarded as unreliable unless repeated noise measurements confirm the stability of the H/V peak amplitude.

5.2 Weigan hill

Weigan hill was severely shattered by seismic shakings during the 2008 Wenchuan sequence (Luo et al., 2014). This motivated the analysis of possible site effects, and the installation of accelerometers at sites Q1, close to the hill top, and Q2, near the foot of the relief. Noise recordings were acquired at these two sites and, additionally, on the top of the hill.

Figure 6 shows the results of the analysis of ambient noise compared to that of seismic event recordings, conducted through the standard spectral ratio (SSR) technique. This technique consists of calculating the spectral ratios, averaged over multiple events, between homologous components of the same event recordings acquired at the study site and at a reference station not affected by amplification (Borcherdt, 1970). The station located in a flat area near the foot of Mount Dong (Q0 in Fig. 1) was used as reference. Directional variations of site response are highlighted by calculating spectral ratios along different horizontal directions spaced by 10° (see polar diagrams in right column of Fig. 6).

The SSR values, already calculated in a previous study (Luo et al., 2014), were reprocessed by calculating spectral ratios of the entire accelerograms and applying to them the same smoothing function (Konno and Ohmachi, 2008) employed for HVNR and HVIP calculations, in order to make SSR more readily comparable with the results of noise analysis. Furthermore, SSR were calculated excluding recordings of weak shocks with a low signal/noise ratio. For the same reason, spectral ratios were not calculated for frequencies < 1 Hz, these being affected by a high noise level in several recordings.

To evaluate the adequacy of Q0 as reference site, we additionally calculated the spectral ratios between horizontal and vertical component of seismic recordings (HVSR: see Lermo and Chávez-García, 1993). The reprocessed data confirmed that Q0 is not completely free from amplification effects (cf., Luo et al., 2014). However, as the amplification occurs only at relatively high frequencies (around 12 Hz) and without a directional character (see the top right polar diagram in Fig. 6), Q0 can be used as reference to recognise the occurrence of directional resonance at lower frequencies.

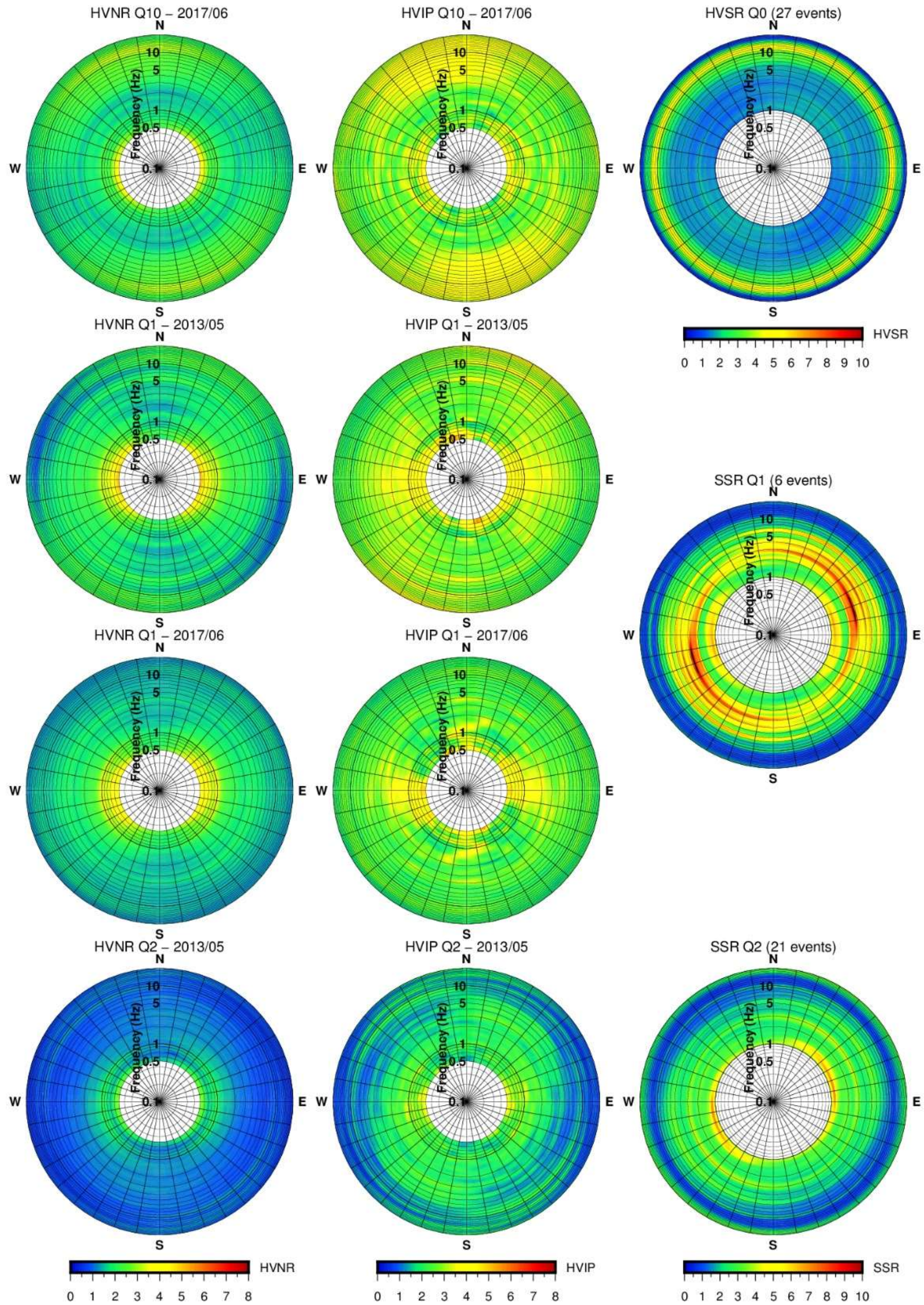

Fig. 6: Polar diagrams showing the values of HVNR (to the left) and HVIP (centre) obtained from noise recordings acquired on Weigan Hill at stations Q10 (on the hill top), Q1 (20 m below the hill top) and Q2 (at the hill foot). At Q1, two distinct noise recordings were acquired in 2013 and 2017, whereas single recordings were carried out at Q2 (2013) and Q10 (2017). For comparison, polar diagrams to the right report standard spectral ratios (SSR) and horizontal-to-vertical spectral ratios (HVSR) calculated from seismic events recorded at Q1, Q2 and Q0. SSR values were calculated comparing recordings of 6 and 21 events at Q1 and Q2, respectively, with those acquired for the same events at the reference station Q0. HVSR values at station Q0 (upper right) were calculated to evaluate its adequacy as reference.

SSR data reprocessing allowed recognition of some previously unrecognized site response features (Luo et al., 2014). In particular, a resonance at a frequency of 1.1 Hz was found at both Q1 and Q2, with a high amplification factor (7.4 at Q1 and 8.2 at Q2) and an approximately ENE orientation (centre and bottom diagrams in the right column of Fig. 6). This resonance effect can be missed when data include recordings of small magnitude events. Such events weakly excite low frequency waves, so that low frequency noise can mask waves generated by earthquakes. Therefore, including a large number of small events in spectral ratio average can considerably “depress” low frequency peaks.

It is noteworthy that not only the frequency, but also the peak amplitude is similar at the two sites (and even slightly higher at Q2, near the base of the hill, than at Q1, near the top). Thus, considering also the high amplification factor, the detected resonance does not appear to be related to a topographic effect, but seems likely controlled by the geology at the scale of the whole relief and, possibly, by the hill size. In addition to the ubiquitous low frequency peak, Q1 shows amplifications in a frequency interval between 2 and 7 Hz, by a maximum factor of 12.3 at 2.7 Hz. These amplifications are likely related to local smaller scale geologic features.

The identification of resonance effects at Q1 and Q2 from ambient noise analysis is problematic, because of the considerable amplification affecting the vertical component of ground motion (see vertical component spectral ratios in Fig. 7). Vertical amplification is considerable around 1 Hz at both Q1 and Q2 sites and is particularly strong at Q1 between 2 and 10 Hz. Such an effect can be responsible for a substantial decrease of the spectral ratios H/V, which makes resonance frequencies practically unrecognisable from HVNR values (see Fig. 7a, c). This effect influences Rayleigh wave ellipticity as well, thus making difficult the recognition of the amplified frequencies. However, at Q2 (Fig. 7c), the weak relative maximum of HVIP at 1 Hz can be correlated to the SSR peak. Moreover, at the site Q10 on the hill top, for which seismic recordings are not available, a peak at the same frequency can be recognized from the HVIP analysis, although it is not very prominent in comparison to the mean level (Fig. 7d). This confirms the ubiquity of 1Hz resonance frequency all over the hill.

More complex appears the site response at Q1. The 1 Hz resonance is not recognisable from the results of the HVIP analysis of the first campaign data (blue curve in Fig. 7b). The relative peak is probably masked within the spectrum trend ascending towards low frequencies, as effect of a strong low frequency background noise that affected the 2013 measurements at both Q1 and Q2 stations (see Fig. 7b-c). A relative maximum, although not so prominent, can be recognised at 1 Hz in the 2017 recording, when the low frequency disturbance was weaker (cyan curve in Fig. 7b); this despite the fact that the site conditions seemingly resulted in a general reduction of Rayleigh wave ellipticity, as also observed at the reference site Qr (see previous section).

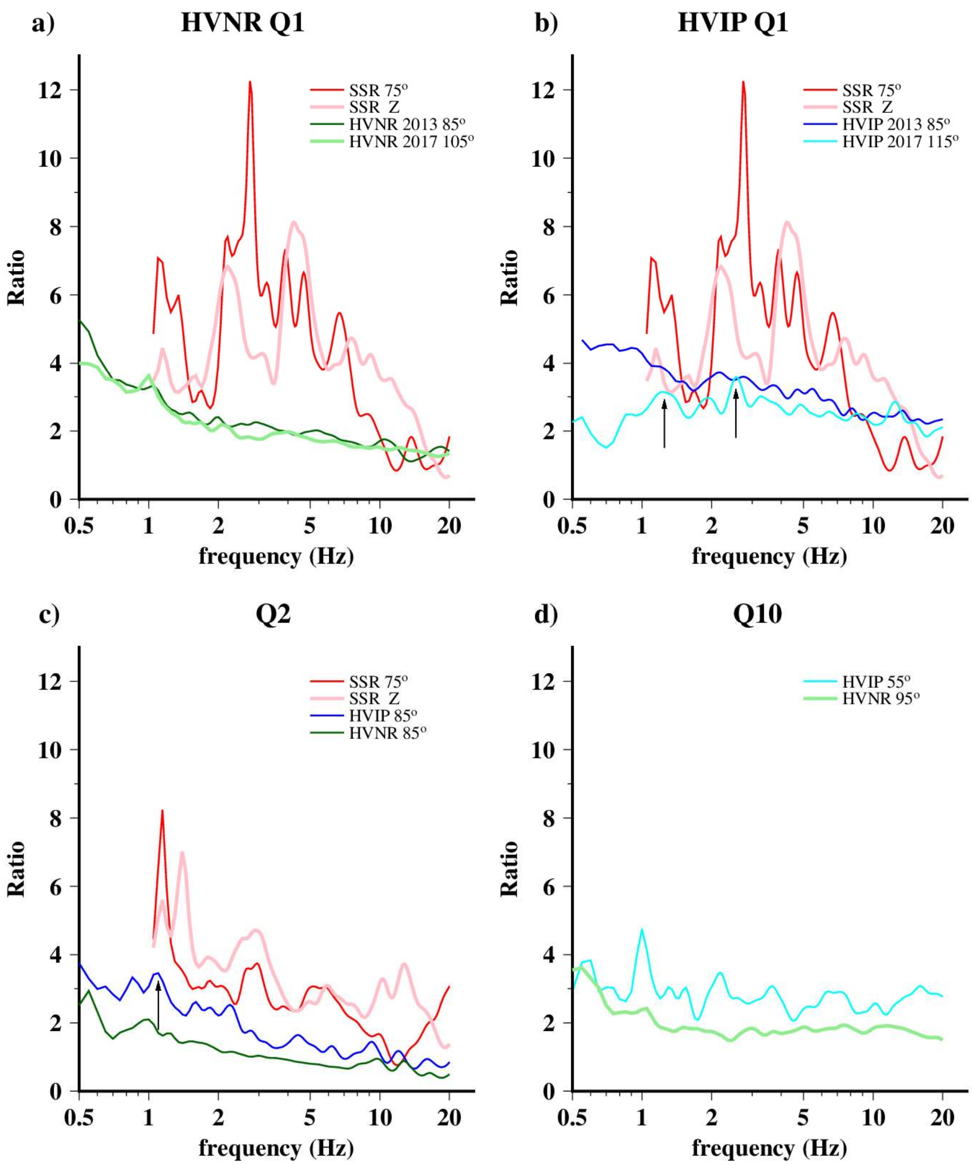

Fig. 7: Curves of HVIP, HVNR and SSR values along directions of their peak values, for stations on Weigan Hill. For Q1 and Q2, SSR values relative to the vertical component are also shown (pink curves). Results of two measurement campaigns are reported for Q1 (see legend). Black arrows mark weak relative maxima correlated to major peaks of SSR curves.

At site Q1, however, the SSR data revealed that the stronger amplifications occur between 2 and 7 Hz, even though the results of noise analyses provided only a very weak evidence of such resonance frequencies. The main reason is that relative maxima of ellipticity, although significant for resonance recognition (H/V > 3 in 2013 and > 2.5 in 2017), do not clearly emerge from the background of ellipticity values external to the 2 - 7 Hz frequency band.

Thus, a coincidence of complex site conditions (vertical component amplification, presence of multiple peak resonance) and unfavourable environmental conditions (occurrence of a strong background signal at frequencies close to those of resonance) can hamper the determination of site response properties from ambient noise analysis only. In such cases, the support of seismic event recordings is needed.

5.3 Mount Dong

The Wenchuan earthquake induced the opening of cracks along the crest of Mount Dong and triggered rock falls. Site response properties were investigated here through the analysis of ambient noise acquired at five sites, named Q3, Q4, Q11, Q5 and Q6 (Figs. 1, 2).

Accelerometer recordings of the 2008 Wenchuan sequence are available only for the Q3 and Q4 stations. Unfortunately, at the time of these recordings, the station Q0, used as reference for the Weigan hill stations, was no longer active and therefore, the seismic recordings at Mount Dong were compared with accelerograms acquired at station Q2. Indeed, the first analyses of Q2 data indicated that the site was not affected by significant amplification (Luo et al., 2014). However, the analyses conducted in the present study revealed that a significant amplification is present, but only at around 1 Hz (see previous section). Furthermore, the number of events recorded at Q2 and at the other two stations is very small (5 and 3 events for Q3 and Q4, respectively). Thus, the SSR results should be regarded with much caution, especially for frequencies around 1 Hz.

Figure 8 shows the results of the noise analyses carried out using the HVNR and HVIP techniques, at stations where also SSR values were available.

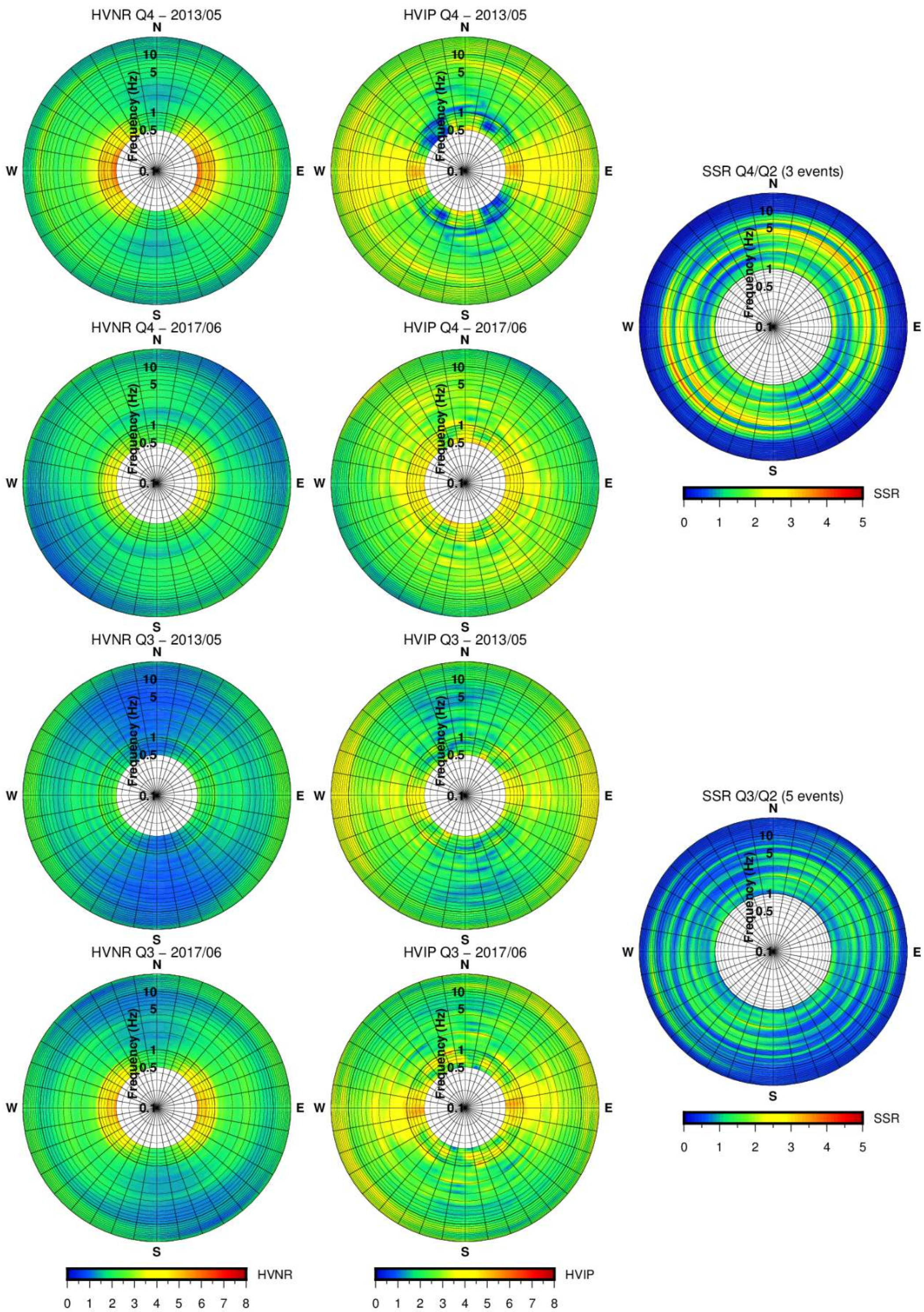

Fig. 8: Polar diagrams of HVNR (to the left) and HVIP (centre) values obtained from noise recordings in 2013 and 2017 on Mount Dong at stations Q4 (middle-lower slope) and Q3 (at the mount foot). For comparison, polar diagrams to the right report standard spectral ratios (SSR) calculated from seismic events using as reference the station Q2 sited at the foot of Weigan Hill.

Overall, the SSR analysis provided much lower values than on Weigan hill. This can be at least in part due to the use of a reference which is not free from some amplification. Thus, these results are to be considered as an estimate of amplification just in relative terms. Nevertheless, the lower SSR values are consistent with the presence of stiffer rocks on Mount Dong. The maximum amplifications were found to reach nearly a factor of 4 at station Q4. In particular, an absolute maximum amplification of 3.9 at 6.9 Hz, and a secondary amplification peak of 3.4 at 4.5 Hz were found to be approximately NE directed. However, the small number of events used for SSR calculation does not allow us to evaluate whether this directivity is due to seismic source properties, or to site effects. At Q3, the maximum amplification factor was so low (i.e. 2.3 at 12.7 Hz) that in general practice it would not be considered diagnostic of amplification occurrence.

The results of the noise analysis at Mount Dong appear dominated by the presence of relatively low frequency components with high H/V ratios and a preferential E-W polarization, with a strong variation between the measurements acquired at different times. The variation indicates that low frequency peaks do not reflect site properties and are likely due to variable conditions of noise generation. However, examining the profile of the Rayleigh wave ellipticity curves estimated through the HVIP technique, some peaks consistently emerge from the results of the two measurement campaigns. These peaks also correlate with the major peaks shown by the SSR values (see Fig. 9). In particular, at Q3, a major peak is observed at a frequency very similar to the SSR maximum (12.9 Hz against 12.7 Hz) and with a higher amplitude (4.2 and 4.0 in HVIP results of 2013 and 2017, respectively, against 2.3 in SSR results). An additional peak consistently shows up at about 1 Hz from both the 2013 and 2017 measurements. This peak does not match any prominent SSR peak, perhaps because all the events used for the SSR analysis were of small magnitude (3.4 at most: see Table 2 in Luo et al., 2014), and, therefore, might not have sufficiently energized such a low frequency.

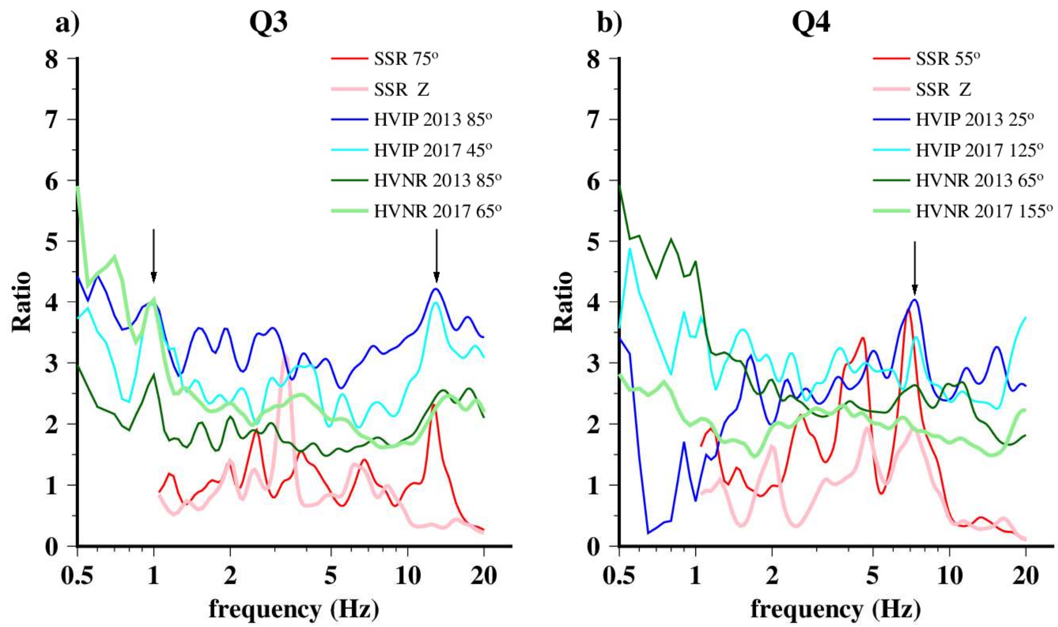

Fig. 9: Curves of HVIP, HVNR and SSR values along the directions of the major peaks for stations Q3 and Q4, located on the middle-lower part of Mount Dong. SSR values relative to the vertical component are also shown (pink curves). Black arrows mark major peaks revealed by noise analysis.

At Q4, the maximum is at a frequency slightly higher than in the SSR values (7.3-7.4 Hz against 6.9 Hz) and has a similar amplitude (4.0 and 3.4 in HVIP results of 2013 and 2017, respectively, against 3.9 in SSR results). This peak emerges less clearly from the measurements of 2017, which were characterised by less favourable environmental conditions for detecting such a small maximum.

It is noteworthy that the direction of HVIP maxima changes from one measurement campaign to the other and does not coincide with those of SSR maxima. This suggests that, at these sites, the weak amplification does not show a pronounced directional character. Furthermore, the Nakamura's technique fails to point out the major resonance frequencies revealed by SSR data, providing spectral ratio curves without any peak significantly exceeding the factor 2, (generally considered a minimum threshold for the identification of amplification conditions using this technique).

For the other measurement points at Mount Dong, seismic data were not available for comparisons. Figures 10 and 11 show the results of analyses of the recordings acquired in the two measurement campaigns at Q5 and in a single campaign at Q6 (2013) and Q11 (2017). Figure 10 reports the polar diagrams of HVIP and HVNR values, whereas a series of curves relative to selected directions are plotted in Fig. 11.

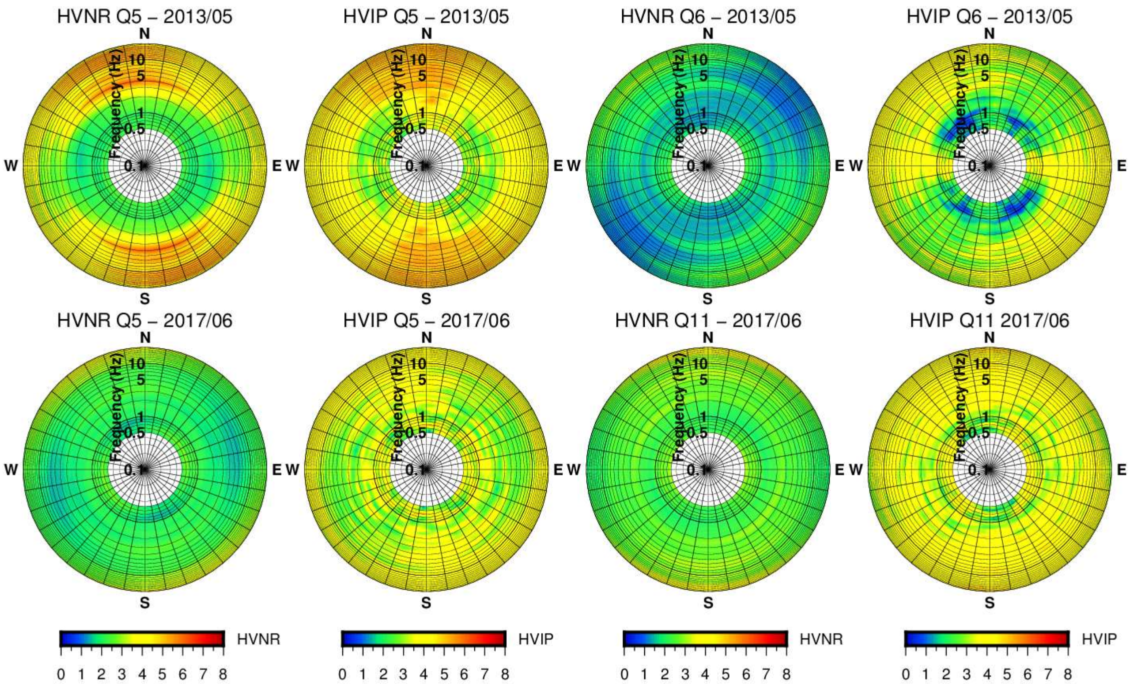

Fig. 10: Polar diagrams of HVNR and HVIP values obtained from noise recordings at Mount Dong stations Q5, Q6 and Q11. At Q5, recordings were acquired both in 2013 and 2017, whereas single recordings were carried out at Q6 (2013) and Q11 (2017).

A clear evidence of site amplification can be recognised only for the site Q5. There the 2013 measurements led to the recognition of a pronounced approximately N-S directed maximum. The maximum showed up in both the HVNR and HVIP analyses, at similar frequencies (4.0 and 3.6 Hz, respectively) and with similar amplitude (6.1 and 5.6, respectively). This site is located exactly on the crest of the Mount Dong ridge, which extends in E-W direction (Figs. 1, 2). Specifically, Q5 is sited on an outcrop of intensely fractured limestone (Fig. 11d). The maximum amplification is transversal to the crest and the fracture system. Secondary peaks with similar N-S orientation are also present at higher frequencies, between 5 and 10 Hz and above 10 Hz (Fig. 11b). Although less pronounced, these maxima can be recognised also in the results of the HVIP analysis of the 2017 recordings (cyan curve in Fig. 11b). However, the peaks at frequencies below 10 Hz cannot be identified from the HVNR analysis of 2017 data.

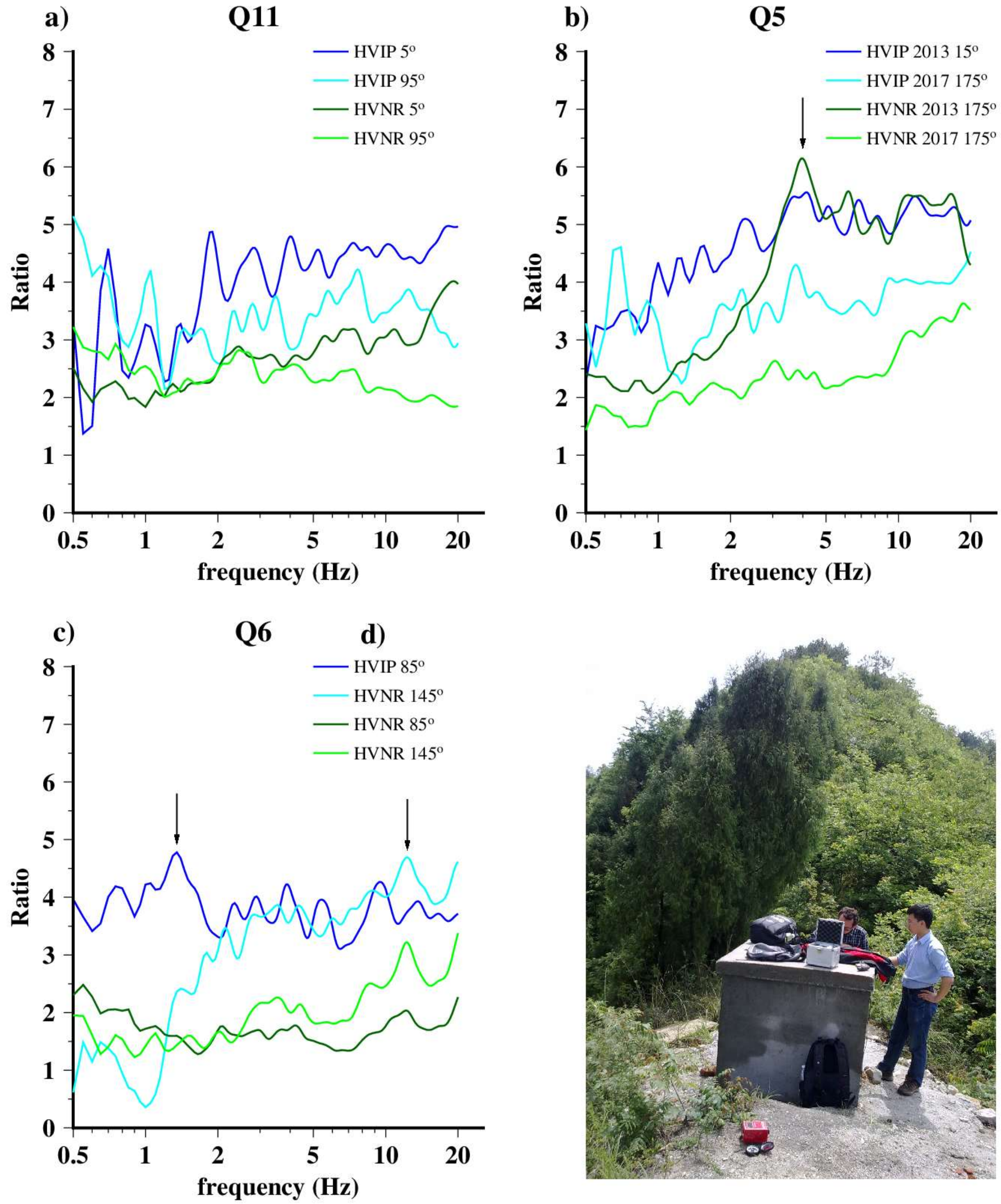

Fig. 11: Curves of HVIP and HVNR values along different directions (see legend) for stations Q11 (a), Q5 (b) and Q6 (c) located in the upper part of Mount Dong. Photo d) shows the site of station Q5: note that the red box in front of the accelerometer station is the tromograph oriented in north-south direction. Black arrows mark major peaks revealed by the noise analysis.

With regard to the other stations, they present a complex pattern of relative maxima without any peaks showing consistent directivity. At Q11, Nakamura's method did not provide significantly high spectral ratios at Q11, except for frequencies close to 20 Hz, with a directional maximum oriented approximately N-S. On the other hand, the HVIP analysis produced some peaks with directional variability, within a relatively wide range of background values of ellipticity. At Q6, the HVIP analysis revealed two prominent directional peaks, one at 1.4 Hz and the other at 12.3 Hz, having different orientations (E-W the former, SE-NW the latter); only the latter is recognizable from the HVNR analysis as well (see Fig. 11c). Overall, since just one noise recording is available for these sites, it remains uncertain whether any of these peaks reflect persistent noise properties related to site response characteristics.

5.4 Mount Shizi

Three measurement points were arranged on Mount Shizi, two of them (Q7 and Q8) at mid-slope altitudes differing few tens of meters, and the other (Q9) near the top of the relief (see Figs. 1, 2). At all these stations, the recordings acquired in 2013 were repeated in 2017. Figures 12 and 13 show the results of the ambient noise analysis.

Polar diagrams (Fig. 12) provide a strong evidence of the directional resonance at site Q7: a pronounced nearly N-S oriented maximum of spectral ratios H/V and of Rayleigh wave ellipticity appears in both 2013 and 2017 recordings. Along the maximum direction, the curves of HVNR and HVIP values consistently show a persistent wide peak around a frequency between 3.9 and 4.7 Hz, possibly composed by the overlapping of more peaks at very close frequencies (Fig. 13b).

The HVNR peak is higher and sharper, but appears less stable in the recordings: in 2013 its amplitude was 10.0 at 4.1 Hz, whereas in 2017 it was reduced by 20% (8.0 at 4.6 Hz). Furthermore, in 2017 this peak is no longer the absolute maximum, being exceeded by a peak of 8.5 at a frequency of 6.1 Hz, (absent in 2013 measurements). Comparatively, ellipticity estimates gave more consistent results in the two recordings, with a H/V maximum of 6.2 at 3.9 Hz in 2013 and of 5.7 at 4.5 Hz in 2017. This confirms the greater stability of the results from the analysis relying only on the Rayleigh wave contribution singled out from the noise recording: it is likely that the larger variation in HVNR peak amplitudes depends on a temporal variation in the relative proportion of different types of waves (e.g., Love waves, which tend to increase the H/V ratios).

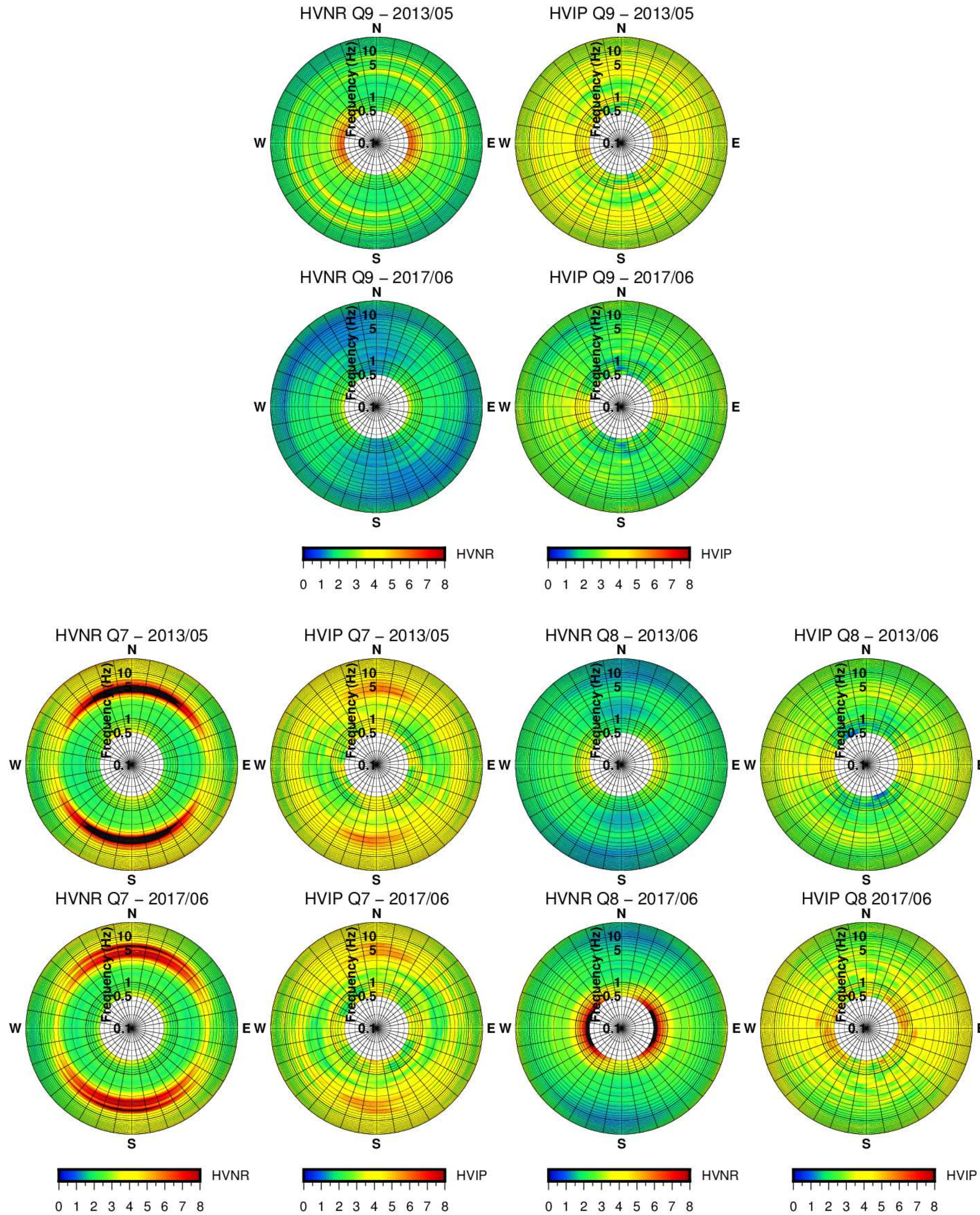

Fig. 12: Polar diagrams of HVNR and HVIP values obtained from noise recordings of the 2013 and 2017 measurement campaigns on Mount Shizi, at stations Q7, Q8 and Q9.

It is noteworthy that Q7 site conditions at Mount Shizi present a certain analogy with site Q5 on Mount Dong: indeed, both sites are located on rocky outcrops and on the crest of ridges elongated approximately in E-W direction, i.e., transversally to the directions of HVNR and HVIP maxima.

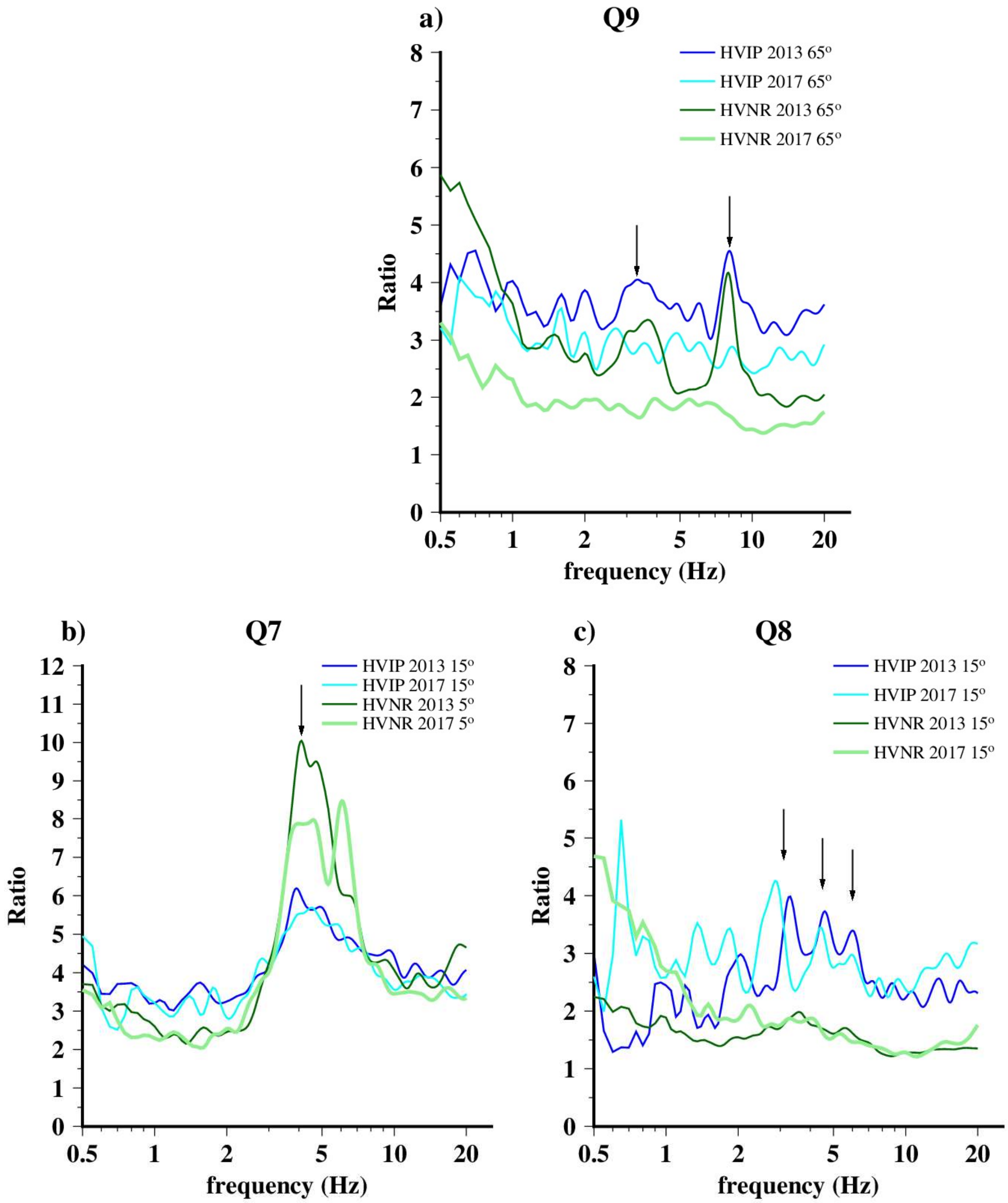

Fig. 13: Curves of HVIP and HVNR values along selected azimuths (see legend) for stations Q9 (a), Q8 (b) and Q7 (c) located on the Mount Shizi. Black arrows mark major peaks revealed by the noise analysis.

At site Q8, located less than 100 m away from Q7, but slightly off the ridge crest, the presence

of amplification conditions is less evident. The polar diagrams are dominated by high values of spectral ratios H/V and Rayleigh wave ellipticity at low frequencies with a preferential E-W polarization (Fig. 12). However, a significant directional peak can be recognized in HVIP values along a direction N15°E. The ellipticity curves in this direction (Fig. 13c) show three peaks in both recordings, with amplitudes of 4.0 at 3.3 Hz, 3.7 at 4.6 Hz and 3.4 at 6.0 Hz (in 2013) and 4.3 at 2.9 Hz, 3.5 at 4.4 Hz and 3.0 at 6.0 Hz (in 2017). Thus, relatively higher ellipticity are present in the same frequency interval of the maximum at Q7, but with smaller amplitude.
The above-mentioned maxima are not recognizable from the HVNR values, which, along the same direction, show only a small increase of spectral ratios H/V not exceeding the threshold of 2. Thus, overall, the presence of directional resonance is probable at this site as well, but its evidence is weaker, possibly in relation to a lower amplification factor.
Finally, the analysis of noise recorded at the site Q9, at the top of Mount Shizi, shows uncertain evidence of site amplification. As in the case of Q8, polar diagrams are dominated by low-frequency E-W oriented maxima of HVNR and HVIP values (Fig. 12), but a couple of directional maxima can be also recognised along a distinct orientation, at least in the 2013 recordings. The major peak is oriented along a N65°E direction, which locally coincides with that of the ridge crest azimuth, and has similar amplitude and frequency in HVNR (4.2 at 8.0 Hz) and in HVIP values (4.5 at 8.1 Hz, Fig. 13a). A secondary maximum is present between 3 and 4 Hz. Both peaks are very subdued in the 2017 HVIP data and cannot be recognized in the 2017 HVNR data. Thus, it is unclear whether such peaks reflect site response properties, which can show up more or less clearly depending on the recordings' environmental conditions more or less favourable to their detection, or are related to changing properties of noise sources.

6. Discussion and conclusions

The 2008 Wenchuan earthquake event demonstrated once again that slope susceptibility to seismically induced landslides is a critical issue for civil protection. This is especially evident in regions where urbanised areas are located at the foot of slopes, whose failure during an earthquake can have disastrous consequences. A thorough evaluation of collateral seismic hazard and the planning of effective countermeasures should take into account the role that seismic shaking amplifications can have in increasing slope susceptibility to landsliding. The relevant information may not be obtained through extensive accelerometer monitoring of marginally stable slopes, because this would require a prolonged employment of costly instrumentation on a large number of slopes and because site response can show sharp variations even within short (tens-hundreds of meters) distances (e.g., Wasowski et al., 2011 and references therein).

The use of techniques based on the analysis of ambient noise recorded for short time by portable lightweight instruments offers an attractive alternative for extensive investigations of slopes' dynamic response to seismic shaking. However, the application of a standard technique of noise analysis (e.g., Nakamura's method), devised for simple sites characterised by flat surfaces and horizontal layering, can be of limited utility. Our earlier studies (Del Gaudio et al., 2008; Del Gaudio, 2017) and this work show that in the presence of geomorphologically complex slopes and sharp lateral lithological heterogeneities, advanced processing techniques should be used to fully exploit the informative potential of noise data.

The case of the hillslopes impending over the urban area of Qiaozhuan, in Qingchuan county, where seismic ground motion data have been collected by a temporary accelerometer monitoring, offered further possibility to test a new method of ambient noise analysis (HVIP) based on the estimate of ellipticity of Rayleigh wave packets identified within noise recordings (Del Gaudio, 2017). The comparative test included also the analysis of data acquired at a reference station located on flat alluvial deposits. The outcomes showed that, while the Nakamura's method provides reliable estimates of resonance frequency related to impedance contrast between a soft surface layer and a stiffer substratum, the interpretation of the curve of spectral ratio H/V in terms of sub-soil velocity, should be dealt with caution even in such simple site conditions. Indeed, the peak amplitude, which in H/V curve inversion constrains the overburden-bedrock impedance contrast and the P-wave velocities within the subsoil model, can show a strong variability. This likely depends on changing conditions of noise wave-field energization and/or seasonal variation of subsoil properties (e.g., water content). Thus, without a check of the peak amplitude variability, interpretation of H/V curves derived from a single noise recordings can be misleading.

In complex site settings (common for landslide-prone slopes), typically characterised by multiple H/V peaks with directional variability, unfavourable environmental conditions can even lead to a reduction of H/V peak amplitude and thus suppress the evidence of site resonance. This is particularly true at sites where vertical component of ground motion is amplified.

Comparatively, the HVIP method, provides more stable results, likely because it "cleans" the ellipticity curve from the effects of changes in noise wave-field composition. In fact, the temporally variable proportion of different wave types results in different contributions to the amplitude of horizontal and vertical motion.

Therefore, the repetition of noise measurements is recommended, possibly after a sufficient time span that implies a variation of noise source characteristics and environmental conditions. This approach is needed to identify, within complex ellipticity curves with multiple peaks, which of them reflects persistent site-specific properties of noise wave-field related to site response characteristics.

The comparison of the seismic recordings processed using the SSR approach with the results of HVIP and HVNR analyses, showed that the new advanced technique is able to point out site resonance properties unrecognisable with the Nakamura's method. This holds if the site is not affected by vertical component amplification. Indeed, the vertical component amplification can considerably reduce not only the spectral ratios H/V, but also the ellipticity peaks and, in such cases, only the seismic recordings can reveal site resonance.

Figure 14 provides an overview of the results of the site response investigations of hillslopes in the peri-urban area of Qiaozhuang. Overall, the analysis of the data derived from the seismic events and noise recordings demonstrates that:

i) Weigan hill is affected by an ubiquitous resonance at 1.1 Hz likely related to geological-structural factors at the scale of the entire relief, and independent of topographic amplification; the hill experiences also amplification effects at higher frequencies, related to local scale site characteristics;

ii) At both Mount Dong and Mount Shizi, the sites on the ridge crest, made of intensely fractured rocks, show a similar resonance pattern with a pronounced directional maxima transversal to the crest and with a similar frequency around 4 Hz; such effect seems to diminish within short distance from the crest edge;

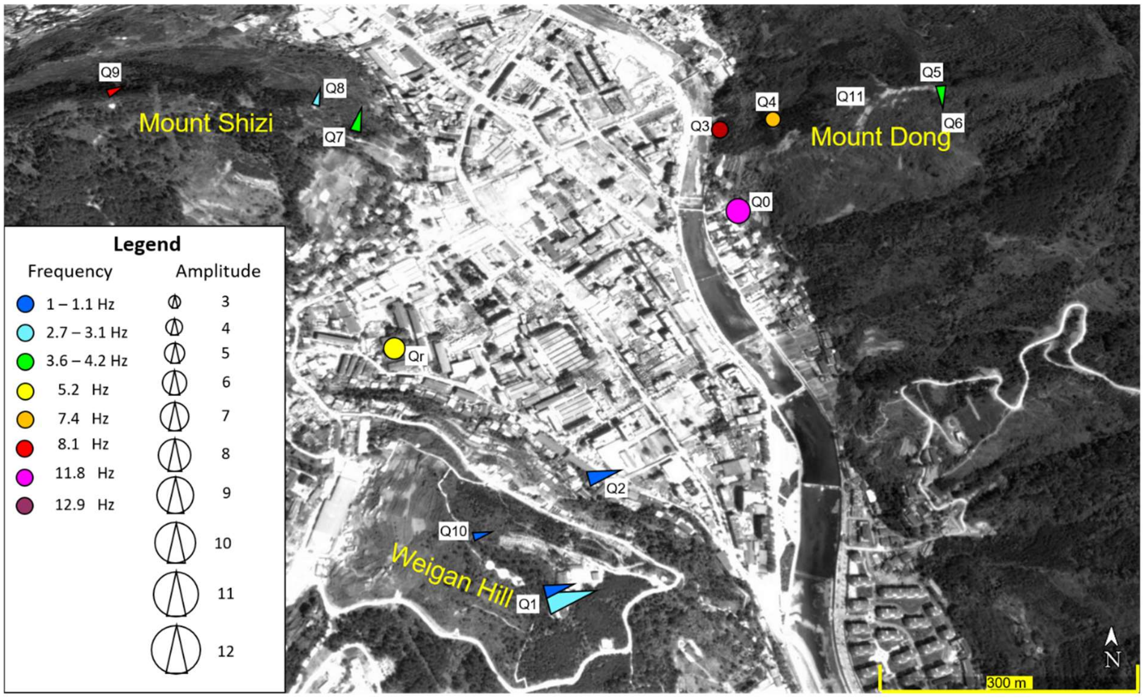

Fig. 14: Resonance frequencies resulting from the analysis of seismic (SSR, HVSR) and ambient noise (HVIP) recordings. Elongated triangles mark orientation of directional resonance, whereas circles indicate the absence of a clear site response directivity. Colours and symbols' sizes are arranged to represent frequency and amplitude of peak values of SSR (Q1, Q2), HVSR (Q0) and HVIP (other stations), respectively (see legend). Note that amplitudes of SSR peaks at Q1 and Q2 are not directly comparable with the H/V values reported for the other stations. Background optical image is from Google Earth^{TM}.

iii) Locally, resonance phenomena appear at higher frequencies, from 7 to 20 Hz, varying from one site to the other, some with a directional character; this could be related to the very local scale geological features.

Our results indicate that both geologic and topographic factors influence the amplification effects detected at Qiaozhuang. Our interpretations are limited in particular by the scarcity of information about the subsurface geology. Nevertheless, the outcomes of this study show that the uppermost parts of peri-urban hills at Qiaozhuang were likely affected by amplified shaking during the 2008 Wenchuan earthquake. This in turn favoured co-seismic slope deformations and failures.

Acknowledgements

Study sponsored by the Chengdu University of Technology (P.R. China) through the Open Fund of the State Key Laboratory of Geohazard Prevention and Geoenvironment Protection with Project No. SKLGP2017K004. Field work was supported also by the funds of the Creative Research Groups of China (Grant No.41521002).

Two anonymous reviewers, with their thoughtful observations and comments, helped us to considerably improve this paper.

References

Bard, P.-Y., 1999. Microtremor measurements: a tool for site effect estimation? In: Irikura, K., Kudo, K., Okada, H., Sasatani, T. (eds), The effects of surface geology on seismic motion, 1251–1279, Balkema, Rotterdam.

Bard, P.Y. and the SESAME Team (2004): Guidelines for the implementation of the H/V spectral ratio technique on ambient vibrations. SESAME European research project WP12 – Deliverable D23.12, 62 pp, ftp://ftp.geo.uib.no/pub/seismo/SOFTWARE/SESAME/USER-GUIDELINES/ SESAME-HV-User-Guidelines.pdf.

Bonnefoy-Claudet, S., Cotton, F., Bard, P.-Y., 2006. The nature of seismic noise wavefield and its implications for site effects studies – A literature review, Earth-Sci. Rev., 79, 205–227.

Borcherdt, R.D., 1970. Effects of local geology on ground motion near San Francisco Bay. Bull. Seism. Soc. Am., 60, 29–61.

Burjánek, J., Gassner-Stamm, G., Poggi, V., Moore, J. R., Fäh, D., 2010. Ambient vibration analysis of an unstable mountain slope. Geophys. J. Int., 180, 820-828

Castellaro, S., Mulargia, F., 2009. VS30 Estimates Using Constrained H/V Measurements. Bull. Seism. Soc. Am., 99, 761–773.

Danneels, G., Bourdeau, C., Torgoev, I., Havenith, H. B., 2008. Geophysical investigation and dynamic modelling of unstable slopes: case-study of Kainama (Kyrgyzstan). Geophys. J. Int., 175, 17-34.

Del Gaudio, V., 2017. Instantaneous polarization analysis of ambient noise recordings in site response investigations. Geophys. J. Int., 210, 443–464, doi: 10.1093/gji/ggx175.

Del Gaudio, V., Coccia, S., Wasowski, J., Gallipoli, M.R., Mucciarelli, M. 2008. Detection of directivity in seismic site response from microtremor spectral analysis. Nat. Hazards Earth Sys. Sci., 8, 751-762.

Del Gaudio, V., Wasowski, J., Muscillo, S., 2013. New developments in ambient noise analysis to characterise the seismic response of landslide prone slopes. Nat. Hazards Earth Sys. Sci., 13, 2075-2087, doi: 10.5194/nhess-13-2075-2013, 2013.

Del Gaudio, V., Muscillo, S., Wasowski, J., 2014. What we can learn about slope response to earthquakes from ambient noise analysis: An overview. Eng. Geol., 182, 182-200.

Fan, X., Juang, H., Wasowski, J., Huang, R., Xu, Q., Scaringi, G., van Westen, C.J., Havenith, H-B. (2018). What we have learned from the 2008 Wenchuan Earthquake and its aftermath: A decade of research and challenges. *Engineering Geology, 241*, 25-32. DOI: 10.1016/j.enggeo.2018.05.004.

Gallipoli, M. R., Lapenna, V ., Lorenzo, P ., Mucciarelli, M ., Perrone, A ., Piscitelli, S., Sdao, F., 2000. Comparison of geological and geophysical prospecting techniques in the study of a landslide in southern Italy. Eur. J. Environ. Eng. Geophys., 4, 117-128.

Harp, E. L., Jibson, R. W., 2002. Anomalous concentrations of seismically triggered rock falls in Paicoma Canyon: are they caused by highly susceptible slopes or local amplification of seismic shaking?. Bull. Seismol. Soc. Am., 92, 3180– 3189.

Havenith, H. B., Jongmans, D. , Faccioli, E., Abdrakhmatov, K., Bard, P.-Y. , 2002. Site effect analysis around the seismically induced Ananevo rockslide, Kyrgyzstan. Bull. Seismol. Soc. Am., 92, 3190-3209.

Jongmans, D., G. Bievre, Renalier, F., Schwartz, S., Beaurez, N., Orengo, Y., 2009. Geophysical investigation of a large landslide in glaciolacustrine clays in the Triéves area (French Alps). Eng. Geol., 109, 45-56.

Liu, G., Li, Y., Cheng, J., Xie, L., 2009. The problem of earthquake fault about Qiaozhuang town in the Qingchuan County after Wenchuan earthquake. J. Mt. Sci. 4, 496–500 (in Chinese).

Luo, Y., Del Gaudio, V., Huang, R., Wang, Y., Wasowski, J., 2014. Evidence of hillslope directional amplification from accelerometer recordings at Qiaozhuang (Sichuan — China). Eng. Geol., 183, 193-207, doi:10.1016/j.enggeo.2014.10.015.

Méric, O., Garambois, S., Malet, J. P., Cadet, H., Gueguen, P., Jongmans, D., 2007. Seismic noise-based methods for soft-rock landslide characterization. Bull. Soc. Geol. Fr., 178, 137-148.

Konno, K., Ohmachi, T., 1998. Ground motion characteristics estimated from spectral ratio between horizontal and vertical components of microtremor. Bull. Seism. Soc. Am., 88, 228-241.

Lermo, J., Chávez-García, F.J., 1993. Site effect evaluation using spectral ratios with only one station. Bull. Seism. Soc. Am., 83, 1574-1594.

Meunier, P., Hovius, N., Haines, J. A., 2008. Topographic site effects and the location of earthquake induced landslides. Earth Planet. Sc. Lett., 275, 221-232.

Moore, J.R., Gischig, V., Burjanek, J., Loew, S., Fäh, D., 2011. Site Effects in Unstable Rock Slopes: Dynamic Behavior of the Randa Instability (Switzerland). Bull. Seism. Soc. Am.,, 101 (6), 3110–3116.

Morozov, I. B., Smithson, S. B. 1996. Instantaneous polarization attributes and directional filtering. Geophysics, 61, 872-881.

Nakamura, Y., 1989. A method for dynamic characteristics estimation of subsurface using microtremor on the ground surface. Q. Report Railway Tech. Res. Inst., 30, 25–33.

Qi, S., Xu, Q., Lan, H., Zhang, B., Liu, J., 2010. Spatial distribution analysis of landslides triggered by 2008.5.12 Wenchuan Earthquake, China. Eng. Geol. 116, 95–108.

Sepúlveda, S. A., Murphy, W., Jibson, R. W., Petley, D. N., 2005. Seismically induced rock slope failures resulting from topographic amplification of strong ground motions: The case of Pacoima Canyon California. Eng. Geol., 80, 336-348.

Sheng, J., Wang, Z., Wang., Z., 2009. Emergency Governance Project Investigation Report of Weiganliang Unstable slope in Qingchuan County of Sichuan Province (in Chinese).

Wang, Y., Luo, Y., Wang, F., Wang, D., Ma, X., Li, S., Deng, X., 2012. Slope Seismic Response Monitoring on the Aftershocks of the Wenchuan Earthquake in the Mianzhu Section. J. Mt. Sci., 9, 523–528, doi: 10.1007/s11629-012-2179-y.

Wasowski, J., Lee, C.T., Keefer, D., 2011. Toward the next generation of research on earthquake induced landslides: Current issues and future challenges, Eng. Geol., 122, 1–8, doi:10.1016/j.enggeo.2011.06.001, 2011.